Inorganica Chimica Acta 549 (2023) 121400

Contents lists available at ScienceDirect

Inorganica Chimica Acta

journal homepage: www.elsevier.com/locate/ica

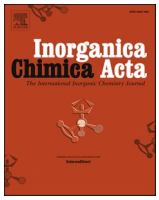

Solvent induced selective response to metal ions of three HNBO-based chemosensors

Daniele Paderni, Daniele Lopez, Eleonora Macedi *, Gianluca Ambrosi, Angela Ricci, Erika Palazzetti, Luca Giorgi, Mauro Formica, Vieri Fusi *

Department of Pure and Applied Sciences, University of Urbino "Carlo Bo", via della Stazione 4, 61029 Urbino, Italy

ARTICLE INFO

Keywords:
Amine ligands
HNBO
Fluorescence
Magnesium
Solvent effect

ABSTRACT

The 2-(2-hydroxy-3-naphthyl)-4-methylbenzoxazole (HNBO) fluorophore has been linked to three different amine scaffolds obtaining three fluorescent chemosensors (**L1**–**L3**). The ESIPT (excited-state intramolecular proton transfer) behavior was investigated in ACN and DMSO by UV–Vis spectrophotometric and spectrofluorimetric measurements, revealing the occurrence of an ESIPT process only in ACN, in the case of **L1** and **L2**, and in both aprotic solvents, besides protic solvents (water and EtOH-water mixture), in the case of **L3**. The emission of **L1**–**L3** is related to the deprotonated form of the ligand. The binding properties of **L1**–**L3** towards Alkali, Alkaline-earth and some transition metal ions were investigated in different solvents by UV–Vis absorption, fluorescence emission and NMR spectroscopies. The fluorescence switches-ON in the presence of selected metal ions, always showing a mechanism different from ESIPT. All **L1**–**L3** show a selectivity for Mg^{2+} in DMSO, while in ACN the selectivity of **L1** and **L2** shifts towards Zn^{2+} and Cd^{2+}. **L3** is also able to respond to Mg^{2+} in other aprotic solvents (THF and dioxane). **L1** and **L3** also showed the ability to signal the presence of metal ions on a paper support (**L1**: Zn^{2+}; **L3**: Zn^{2+}, Cd^{2+} and Mg^{2+}). Therefore, **L3** revealed able to signal the presence of Mg^{2+} both in solution, in different solvents, as well as on a paper support.

1. Introduction

The research of new chemosensors able to selectively bind and signal the presence of specific metal ions in samples of biological and environmental relevance is an always growing field. Metal cations such as Mg^{2+}, Ca^{2+} and Zn^{2+} play crucial roles in the human physiology. Mg^{2+} is indeed involved in many cellular processes, being important for the activity of enzymes, receptors and ionic channels and for the bone metabolism [1–9]. As a consequence, inadequate levels of Mg^{2+} result in several disorders, such as migraine, chronic pain, epilepsy, hypocalcaemia, hypertension, renal and gastrointestinal losses, Alzheimer's, Parkinson's, stroke, anxiety, depression, bone formation decline, diabetes mellitus type 2 and cancer [10–15]. On the other hand, excessive levels of Mg^{2+} that could come from contamination of food or water supplies with magnesium salts, are known to cause hypermagnesemia, nausea, hypotension and diarrhea [16,17].

For this reason, a growing attention is being devoted to the detection of Mg^{2+} in samples of different nature. Fluorescent probes, due to their reliability, simplicity, velocity, sensitivity, selectivity and real-time detection represent a valid alternative to more expensive and less simple handling instrumental analytical techniques such as atomic absorption spectrometry with flame (F-AAS) or electrothermal (ETA-AAS) atomization, null-point titration techniques and NMR [17–20].

Many chemosensors reported so far, however, are not able to discriminate between Mg^{2+} and other metal cations such as Ca^{2+} and Zn^{2+} [21–32]. Selective fluorescent systems able to distinguish especially between Mg^{2+} and Ca^{2+} are therefore highly desirable, both for biological and environmental samples.

Recently, a new series of ligands containing the 2-(2-hydroxy-3-naphthyl)-4-methylbenzoxazole (HNBO) fluorophore linked to polyamine scaffolds was synthesized and investigated (N-(2-(2′-hydroxy-3′-naphthyl)benzoxazol-4-ylmethyl)-N,*N*-dimethylamine, **L1**; N-(2-(2′-hydroxy-3′-naphthyl)benzoxazol-4-ylmethyl)-N,N′,N′-trimethylethylendiamine, **L2**; N,N′-bis(2-(2′-hydroxy-3′-naphthyl)benzoxazol-4-ylmethyl)-N,N′-dimethylethylendiamine, $\mathbf{L_A}$) (Fig. 1): the most complex ligand within the series ($\mathbf{L_A}$), containing two HNBO units, revealed as the most promising chemosensor in terms of fluorescence response to Mg^{2+} in DMSO [33]. Notably, $\mathbf{L_A}$ showed the highest emission increase upon the

* Corresponding authors.
E-mail address: vieri.fusi@uniurb.it (V. Fusi).

https://doi.org/10.1016/j.ica.2023.121400
Received 31 October 2022; Received in revised form 11 January 2023; Accepted 16 January 2023
Available online 21 January 2023

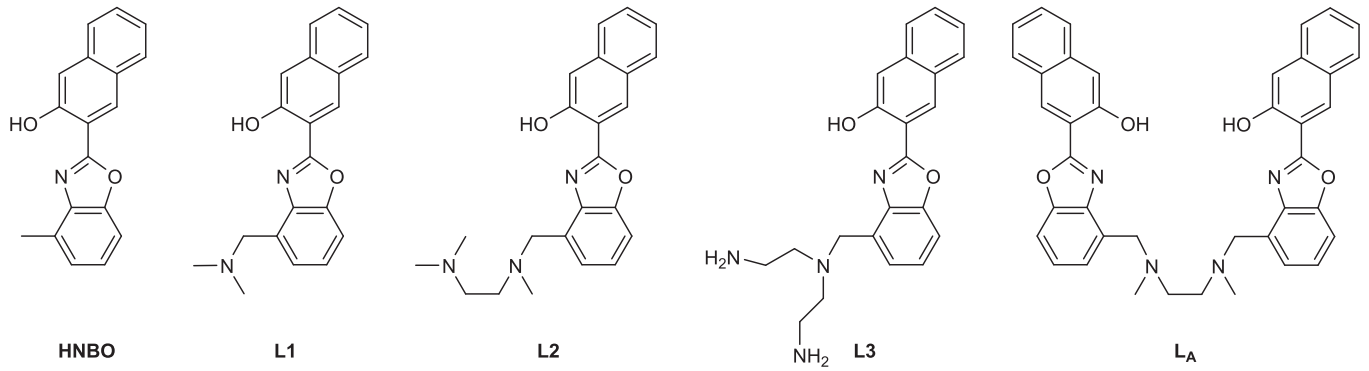

Fig. 1. Molecular structures of compounds HNBO, **L1**, **L2**, **L3** and $\mathbf{L_A}$.

addition of Mg^{2+}, ascribable to a chelation enhancement of the fluorescence (CHEF) effect, considering all Alkali, Alkaline-earth (A, AE) and some transition metal ions (Zn^{2+}, Cd^{2+} and Pb^{2+}) [33]. Previously, the HNBO fluorophore was inserted in ligands that showed the ability to bind Zn^{2+} and Cd^{2+} [34,35], so **L1**, **L2** and $\mathbf{L_A}$ are, to the best of our knowledge, the first HNBO-molecules able to selectively respond to Mg^{2+}.

In this study, the family of HNBO-based molecules has been expanded by synthesizing a new ligand where a HNBO moiety is linked to the *N,N*-bis(2-aminoethyl)amine fragment to obtain the open chain ligand **L3** (*N*-(2-(2′-hydroxy-3′-naphthyl)benzoxazol-4-ylmethyl)-*N,N*-bis(2-aminoethyl)amine). In the previous paper, it has been ascertained that the sole HNBO fluorophore does not respond to any of the tested metal cations [33]. In other words, the conjugation with an amine fragment is necessary to obtain a fluorescence response to a metal cation. Herein, moving from **L1** to **L2** to **L3** the aliphatic structure has been made more and more complex, by increasing the number of nitrogen atoms and the degree of branching. As possible ESIPT (excited-state intramolecular proton transfer)-based sensors, the free ligands were analyzed in different solvents and their acid-base behavior was also investigated. To ascertain if the binding properties of **L1**, **L2** and **L3** towards A, AE and some transition metal ions may be affected by a solvent change [36,37], UV–vis spectrophotometric and spectrofluorimetric measurements in different solvents were performed, revealing different selectivity for metal cations in different conditions. NMR analyses were also performed to acquire more information about the complex formation.

Finally, the binding performance of the three chemosensors towards selected metal ions was assessed also on a paper support, trying to develop an easy and fast qualitative method to reveal the presence of the target cations in solution samples.

2. Experimental

2.1. Instruments and materials

All chemicals were purchased in the highest quality commercially available. The solvents were RP grade, unless otherwise indicated, and used without further purification. All reactions involving moisture-sensitive reagents were carried out under a nitrogen atmosphere using standard vacuum line techniques and glassware that was flame-dried before use.

Elemental analysis was performed with a Thermo Finnigan Flash 1112 EA CHN analyser.

Mass spectra were performed with an Agilent 1200 Series HPLC system equipped with a binary pump and a C18 column (Phenomenex Synergi™ 4 μm Fusion-RP 80 Å, LC Column 50 × 2 mm, Ea), coupled to a SCIEX mod. API 4000 QqQ triple quadrupole mass spectrometer with ESI source.

Pictures depicted in Figs. 6b, 11b, 13 were taken with the digital camera of a common smartphone.

More details about UV–vis and NMR measurements and paper strip tests are reported in the Supplementary material.

3. Results and discussion

3.1. Synthesis

Ligands **L1** and **L2** were synthesized as previously reported [33].

Ligand **L3** was synthesized by adapting a known procedure to link a HNBO moiety to a secondary amine [35] (Fig. 2). The methoxymethyl (MOM)-protected and brominated compound **1** [35] was coupled in DMF with *N,N*-bis(2-phthalimidoethyl)amine **2** [38] in the presence of sodium carbonate as a base, to give the fully protected intermediate **3**. The *N*-phthaloyl groups were then removed using hydrazine in EtOH

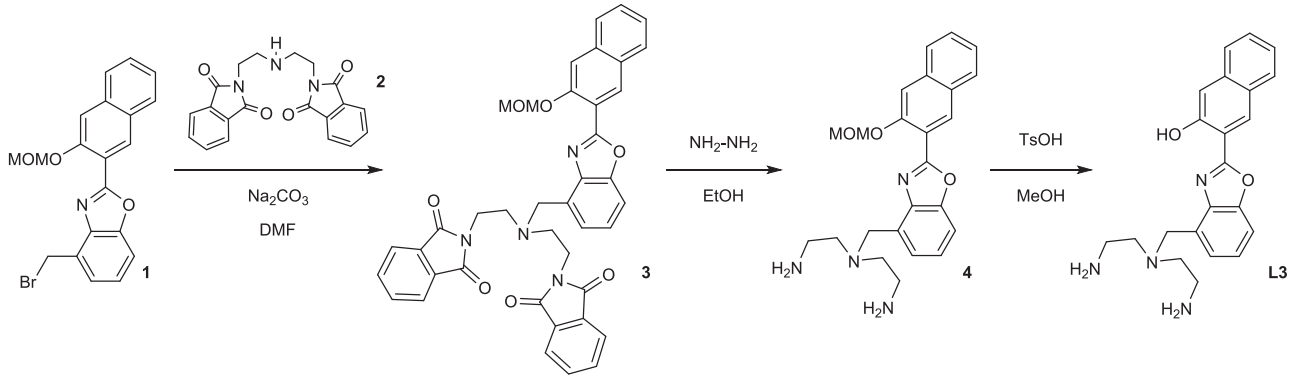

Fig. 2. Synthetic pathway to **L3**.

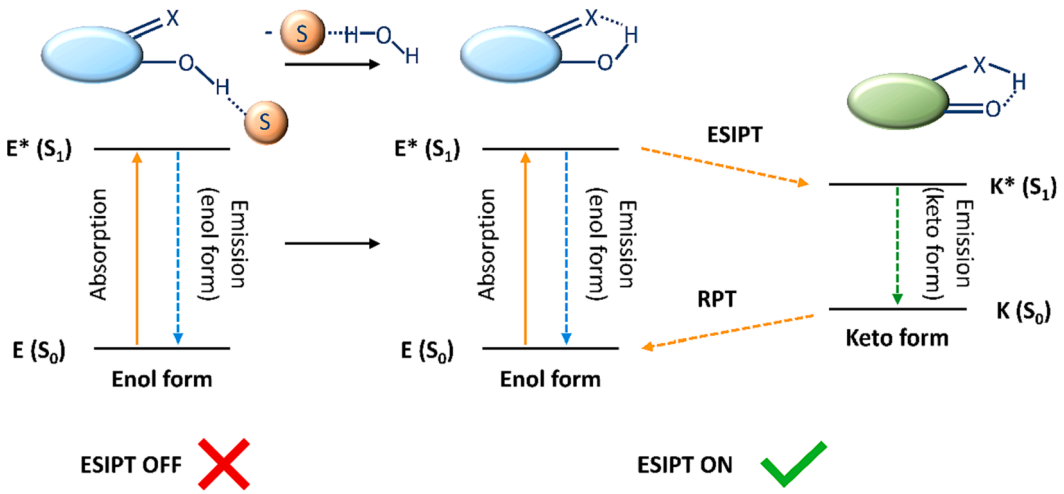

Fig. 3. Mechanism of ESIPT-based fluorescent chemosensors (S = solvent).

affording (**4**) as an orange solid, while the naphthol group was deprotected by using *p*-toluenesulfonic acid (TsOH) in MeOH obtaining **L3**, which was further purified as hydrochloride salt.

Specific details about the synthetic procedures are reported below.

*2-(2-Methoxymethyloxy-3-naphthyl)-4-[N,N,-bis(2-phthalimidoethyl) aminomethyl]benzoxazole (**3**)*

To a dry dimethylformamide (DMF) solution (80 cm^3) of *N,N*-bis(2-phthalimidoethyl)amine (**2**) [38] (1.4 g, 3.8 mmol) containing Na_2CO_3 (2.4 g, 22.8 mmol), a solution of **1** [35] (1.5 g, 3.8 mmol) dissolved in 80 cm^3 of dry DMF was added dropwise within 1 h under nitrogen at room temperature. The reaction mixture was stirred at 40 °C for 16 h, then the desired product was precipitated by slowly addition of cold water. The solid was then recovered by filtration, dried in vacuum at room temperature and purified by column chromatography on silica gel (CH_2Cl_2/hexan, 1:1) to obtain **3** as a yellow solid (1.3 g, 1.9 mmol, y = 50 %).

^{1}H NMR (DMSO-d_6): δ = 2.80 (4H, t, J = 6.0 MHz), 3.75 (4H, t, J = 6.0 MHz), 4.11 (2H, s), 5.45 (2H, s), 6.91 (1H, t, J = 8 MHz), 7.07 (1H, d, J = 7.2 MHz), 7.50 (2H, m), 3.50 (3H, s), 7.62 (1H, td, J^4 = 1.2 MHz, J^3 = 7.6 MHz), 7.70 (1H, s), 7.67 (4H, m), 7.78 (4H, m), 7.92 (1H, d, J = 8 MHz), 8.07 (1H, d, J = 8 MHz), 8.63 (1H, s) ppm; ^{13}C NMR (DMSO-d_6): δ = 35.96, 51.68, 51.49, 56.49, 95.32, 109.45, 111.85, 118.53, 123.16, 125.18, 125.55, 127.19, 128.57, 128.88, 129.01, 130.95, 132.11, 132.57, 134.53, 135.63, 141.32, 150.30, 152.57, 161.00, 168.15 ppm.

*2-(2-Methoxymethyloxy-3-naphthyl)-4-[N,N,-bis(2-aminoethyl) aminomethyl]benzoxazole (**4**)*

To a solution of hydrazine monohydrate (1.3 cm^3, 28 mmol) in 120 cm^3 EtOH was added dropwise a solution of **3** (1.9 g, 2.8 mmol) in 10 cm^3 $CHCl_3$. The reaction mixture was stirred at room temperature for 30 h, then evaporated under vacuum. The residue was suspended in 20 cm^3 $CHCl_3$, the orange solid was filtered off and the solution was evaporated under vacuum. The crude product (1.1 g, 2.6 mmol, y = 92 %) has been used for the next step without any further purification.

^{1}H NMR ($CDCl_3$): δ = 2.63 (4H, t, J = 6 MHz), 2.84 (4H, t, J = 6 MHz), 3.59 (3H, s), 4.04 (2H, s), 5.46 (2H, s), 7.33 (2H, m), 7.42 (1H, td, J^4 = 1.2 MHz, J^3 = 4.8 MHz), 7.53 (2H, m), 7.59 (1H, s), 7.78 (1H, d, J = 8 MHz), 7.91 (1H, d, J = 8 MHz), 8.61 (1H, s) ppm; ^{13}C NMR ($CDCl_3$): δ = 39.53, 53.88, 56.43, 56.71, 95.30, 109.43, 111.54, 118.46, 141.24, 135.56, 132.53, 131.78, 124.72, 124.88, 125.01, 126.85, 128.20, 128.60, 128.69, 150.87, 152.67, 161.42 ppm.

*N-(2-(2′-hydroxy-3′-naphthyl)benzoxazol-4-ylmethyl)-N,N-bis(2-aminoethyl)amine (**L3**)*

Compound **4** (1.1 g, 2.6 mmol) was dissolved in MeOH (100 cm^3) and added dropwise of a solution of *p*-toluenesulfonic acid (TsOH, 2.2 g, 11.7 mmol) in MeOH (20 cm^3) at room temperature. The reaction mixture was stirred at room temperature and the progress of the reaction was monitored by TLC (SiO_2, CH_2Cl_2): following the disappearance of **4**, the reaction mixture was evaporated under vacuum and the residue was dissolved in CH_2Cl_2 (10 cm^3) and washed twice with a saturated K_2CO_3 aqueous solution (20 cm^3). The organic phase was dried on Na_2SO_4, filtered and evaporated under vacuum. The solid was dried under vacuum at room temperature to give **L3** as a white solid (0.65 g, 1.7 mmol, y = 65 %).

The pure **L3** was obtained as hydrochloride salt (**L3·3HCl**) by the addition of a 10 % ethanolic solution of HCl to an ethanolic solution (5 cm^3) of the crude, obtaining 0.73 g (1.5 mmol, y = 57 %).

MS *m/z* ESI ($M + H^+$): 377.20; ^{1}H NMR (D_2O, pH 2): δ = 2.77 (4H, t, J = 6.2 MHz), 3.07 (4H, t, J = 6.2 MHz), 3.76 (2H, s), 7.07 (1H, s), 7.15 (1H, d, J = 7.5 MHz), 7.22 (1H, t, J = 7.4 MHz), 7.32 (2H, m), 7.43 (1H, d, J = 8.3 MHz), 7.52 (1H, d, J = 8.1 MHz), 7.67 (1H, d, J = 8.2 MHz), 8.23 (1H, s) ppm (Fig. S1); ^{13}C NMR (D_2O, pH 2): δ = 33.88, 49.50, 52.78, 110.85, 111.57, 113.35, 118.10, 124.53, 126.06, 126.62, 127.11, 128.22, 128.52, 128.90, 129.67, 135.83, 139.83, 148.99, 151.64, 162.37 ppm (Fig. S1); Anal. for: $C_{22}H_{27}Cl_3N_4O_2$ (485.83), Calc. C 54.39, H 5.60, N 11.53; Found C 54.1, H 5.7, N 11.4.

3.2. Solution studies on the free ligands

3.2.1. ESIPT behavior of free ligands in different solvents

Fluorescent molecular sensors or chemosensors are probes able to change their emission properties in the presence of target analytes; several fluorescence mechanisms can be involved in the signaling processes, mainly PET (Photoinduced Electron Transfer), FRET (Förster Resonance Energy Transfer) and ICT (Internal Charge Transfer), although others can be mentioned; among them, the ESIPT (excited-state intramolecular proton transfer) mechanism could also be exploited using suitable fluorophores. Molecules that can exhibit ESIPT fluorescence feature an intramolecular hydrogen bonding interaction between a hydrogen bond donor (–OH and NH_2) and a hydrogen bond acceptor (=N– and C=O) [39]. During ESIPT, a four-level photochemical process occurs: starting from an enol (E) form, an electronic redistribution takes place upon photoexcitation. The resulting greater acidity of the H bond donor and increased basicity of the H bond acceptor within the E form favor an extremely fast enol to keto (K) phototautomerization ($k_{ESIPT} > 10^{12}$ s^{-1}). The excited state enol form (E*) rapidly converts into its excited keto form (K*), that decays radiatively to its electronic ground state (K), followed by a reverse proton transfer (RPT) to give back the original E form [39] (Fig. 3).

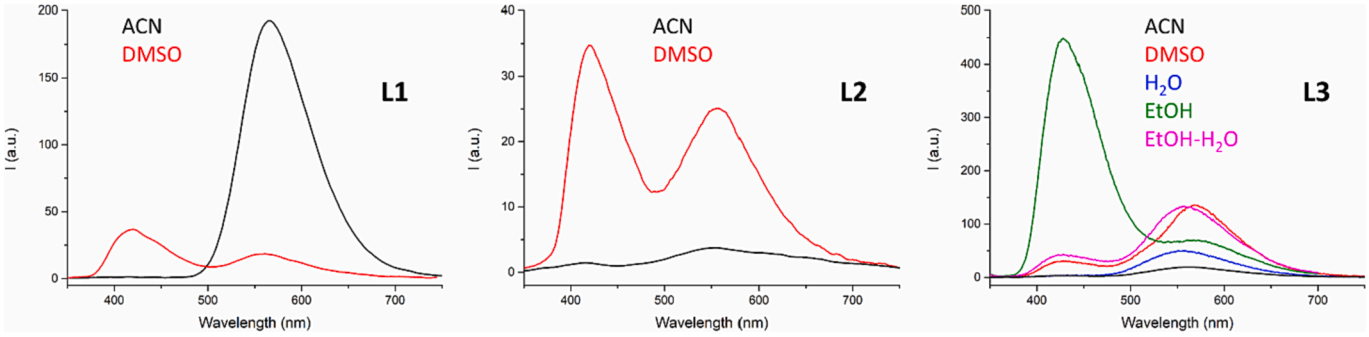

Fig. 4. Emission spectra of **L1**, **L2** and **L3** in different solvents (black line: ACN; red line: DMSO; blue line: water (HEPES pH 7.4), green line: EtOH; magenta line: EtOH + 10 % H_2O). [**L**] = $1.0{\cdot}10^{-5}$ mol/dm^{-3}; λ_{ex} = 317 nm (ACN, EtOH, EtOH-H_2O, H_2O (HEPES pH 7.4)), 320 nm (DMSO); λ_{em}: **L1**: 566 nm (ACN), 420 nm (DMSO); **L2**: 552 nm (ACN), 420 nm (DMSO); **L3**: 561 nm (ACN), 569 nm (DMSO), 554 nm (H_2O), 429 nm (EtOH), 557 nm (EtOH-H_2O). (For interpretation of the references to color in this figure legend, the reader is referred to the web version of this article.)

The ESIPT emission could be greatly affected by the presence of polar and H-bonding solvents, resulting in a restricted ESIPT process and lack of keto (K*) emission due to unavailability of exchangeable protons following H bond formation [40]. The addition of a variable amount of water to a H-bonding solvent could however result in a shift towards the keto form, due the H-bond between the solvent and H_2O becoming prominent over that between the solvent and the fluorophore, releasing the latter from the hydrogen bonding and enabling the ESIPT process [40] (Fig. 3). For this reason, as possible ESIPT-based fluorophores, the free HNBO-containing ligands were analyzed by spectrophotometric and spectrofluorimetric measurements in different solvents. Due to solubility issues, **L1** and **L2** were only studied in DMSO and ACN, while **L3** was studied also in water (HEPES buffer pH 7.4), EtOH and a mixture EtOH-10 % water (HEPES pH 7.4).

All ligands show in ACN (λ_{ex} = 317 nm) an intensity of the keto band (lower energy) higher than the enol band (higher energy), suggesting the occurrence of an ESIPT process (Fig. 4, black lines). Probably, the –OH naphthol group is not stabilized by the formation of hydrogen bond with the ACN molecules.

In DMSO (λ_{ex} = 320 nm), both **L1** and **L2** show the enol band higher than the keto band (Fig. 4, red lines): this suggests that the ESIPT process is prevented, probably due to a possible interaction between the –OH naphthol group and the solvent molecules that make unavailable the exchangeable proton. In other words, the employment of a more basic solvent, also providing a higher number of donor atoms [41], makes the intensity of the enol emission becoming stronger compared to the keto form.

In the case of **L3** in DMSO, similarly to ACN, the band attributed to the keto form is more intense than that of the enol form (Fig. 4). An ESIPT process thus occurs in this molecule in both aprotic solvents, notwithstanding their different basicity [41]. A similar behavior is notably observed also in water (HEPES pH 7.4; λ_{ex} = 317 nm) and in a

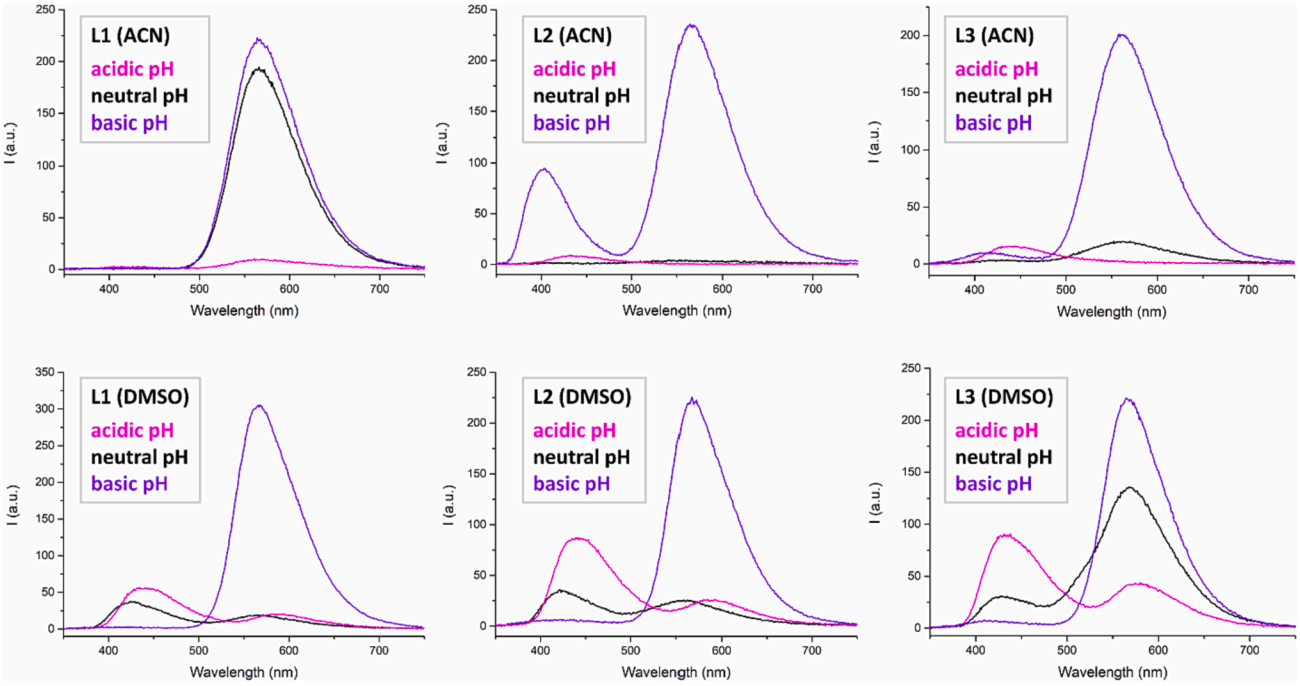

Fig. 5. Emission spectra of **L1**, **L2** and **L3** in ACN (top) and DMSO (bottom) at different pH fields. [**L**] = $1.0{\cdot}10^{-5}$ mol/dm^{-3} DMSO + 1.0 % H_2O; $I = 1.0{\cdot}10^{-3}$ mol/dm^{-3} NMe_4Cl. λ_{ex}: 318, 317, 322 nm (ACN, at acidic, neutral, basic pH field, respectively); 322, 320, 330 nm (DMSO, at acidic, neutral, basic pH field, respectively). λ_{em}: 568, 566, 564 nm (**L1**, ACN, at acidic, neutral, basic pH field, respectively); 441 + 588, 426 + 565, 566 nm (**L1**, DMSO, at acidic, neutral, basic pH field, respectively); 432, 559, 403 + 564 nm (**L2**, ACN, at acidic, neutral, basic pH field, respectively); 441 + 591, 423 + 557, 567 nm (**L2**, DMSO, at acidic, neutral, basic pH field, respectively); 444, 562, 413 + 562 nm (**L3**, ACN, at acidic, neutral, basic pH field, respectively); 431 + 580, 429 + 569, 565 nm (**L3**, DMSO, at acidic, neutral, basic pH field, respectively).

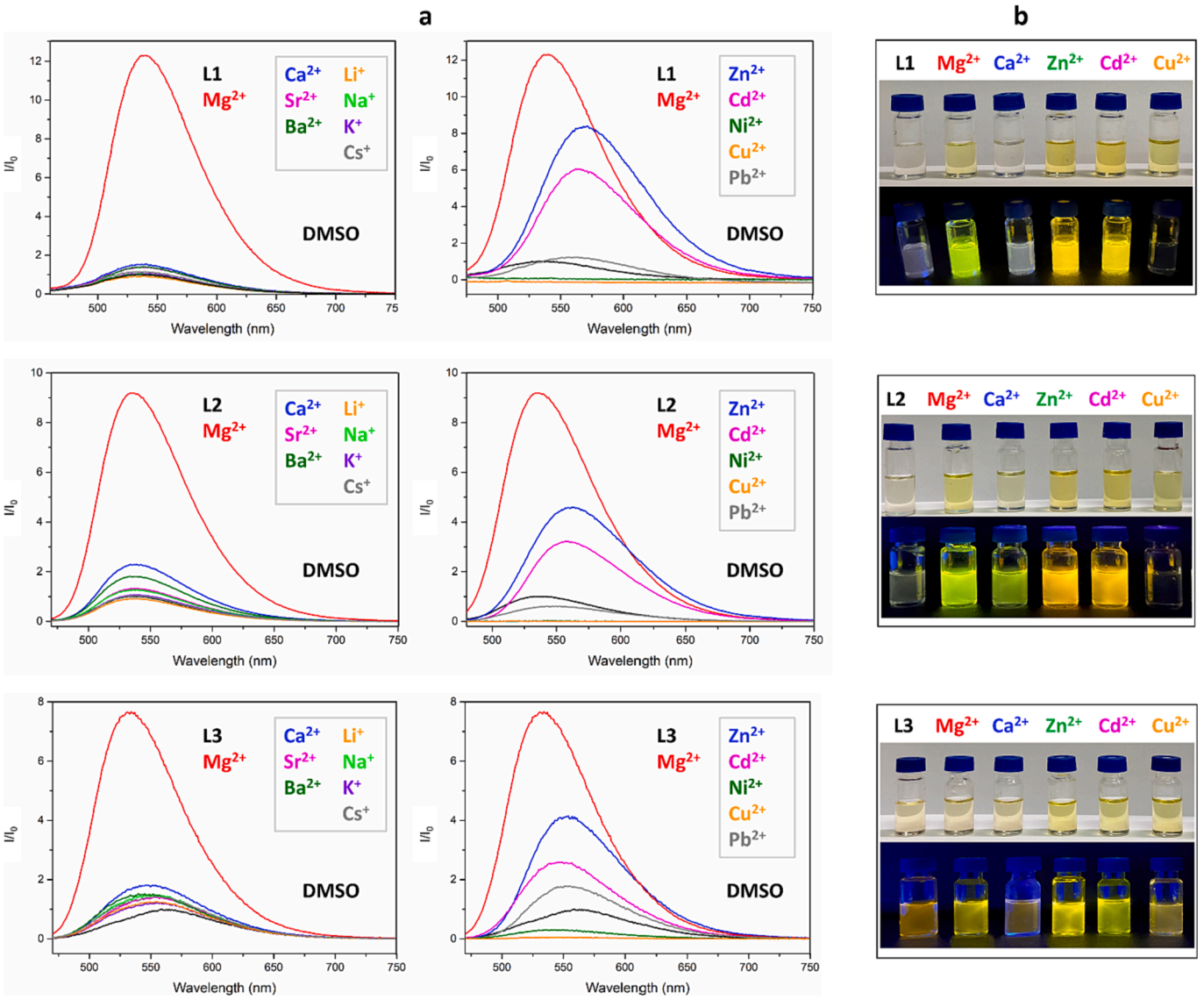

Fig. 6. a) Emission spectra of **L1**–**L3** upon the addition of 1 equiv. of A, AE and transition metal ions in DMSO. b) Color change (top) and enhancement of the fluorescence under a 360 nm UV lamp (bottom) of **L1**, **L2** and **L3** DMSO solutions before and after the addition of 1 equiv. of Mg^{2+}, Ca^{2+}, Zn^{2+}, Cd^{2+}, Cu^{2+}. [**L**] = $1.2{\cdot}10^{-5}$ mol/dm^{-3} DMSO + 1.0 % H_2O; $I = 1.2{\cdot}10^{-3}$ mol/dm^{-3} NMe_4Cl. λ_{ex} = **L1**, **L2**: 440 nm; **L3**: 450 nm (except for Ni^{2+}: 462 nm); λ_{em}: **L1** = 536 nm, + Mg^{2+} = 540 nm, + A, AE = 536 nm, + Zn^{2+} = 570 nm, + Cd^{2+} = 566 nm, Pb^{2+} = 561 nm; **L2** = 534 nm, + Mg^{2+} = 536 nm, + A, AE = 536 nm, + Zn^{2+} = 562 nm, + Cd^{2+} = 559 nm; **L3** = 562 nm, + Mg^{2+} = 532 nm, + A, AE = 552 nm, + Zn^{2+} = 553 nm, + Cd^{2+} = 548 nm, Pb^{2+} = 553 nm.

mixture EtOH-10 % water (HEPES pH 7.4; λ_{ex} = 317 nm), while a much higher enol band compared to the keto band is observed in EtOH (λ_{ex} = 317 nm) (Fig. 4): it can be hypothesized that in the case of **L3** the H-bond formation between the organic solvent and water is favored compared to the interaction between the chemosensor and the organic solvent, enabling the ESIPT process (*vide supra*).

Moreover, no significant variations in the UV–Vis absorption spectra of **L1**, **L2** and **L3** were observed in the different solvents (Fig. S2), suggesting the presence of only one form in the ground state for each ligand.

3.2.2. *Acid-base spectrophotometric behavior of the ligands in different solvents*

The acid-base behavior of **L1**, **L2** and **L3** was spectrophotometrically investigated in both ACN and DMSO, by adding 0.1 mol dm^{-3} TMAOH or HCl to the solutions.

The absorption spectra of **L1**–**L3** in both ACN and DMSO in the presence of a stoichiometric amount of TMAOH mainly show two intense bands and a shoulder, as reported in Table S1.

UV–Vis absorption experiments at different field of pH showed quite similar behaviors for all ligands in both tested solvents, while some differences can be found in the emission spectra. Moving from an acidic to a neutral environment, a small variation of the absorption in the 300–350 nm range was observed while, in a basic environment, a deep modification of the 300–350 nm region along with the appearance of a new absorption band at lower energy attributed to the deprotonation of the naphthol group were observed (Fig. S3).

As for the emission spectra, in an acidic environment all ligands are very low emissive in ACN (λ_{ex} 318 nm), with the enol band prevailing over the keto band, in the case of **L2** and **L3**, while the opposite is observed in the case of **L1** (Fig. 5, top; magenta lines). For all ligands a TICT (twisted intramolecular charge transfer) mechanism could be hypothesized to quench the emission of the enol or keto forms, since a PET effect, with the amine functions being protonated in this pH field, can be ruled out [33]. In DMSO a scarce but not negligible emission of the enol form of all ligands is observed (λ_{ex} 322 nm): it can be hypothesized that, notwithstanding the ESIPT suppression, the two aromatic systems lie on

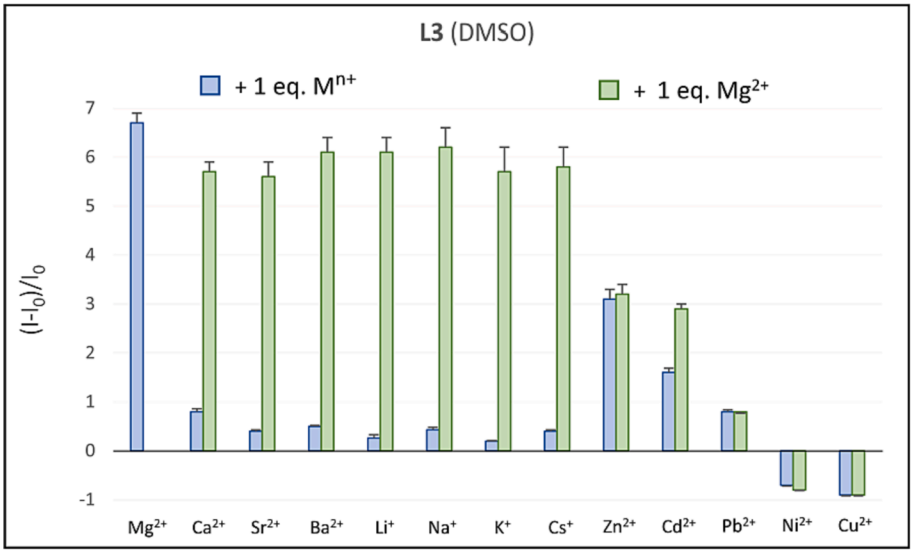

Fig. 7. Normalized maximum fluorescence emission of **L3** upon addition of 1 equiv. of A, AE and transition metal ions (blue bars) and following further addition of 1. equiv. of Mg^{2+} (green bars). [**L**] = $1.2{\cdot}10^{-5}$ mol/dm^{-3} DMSO + 1.0 % H_2O; I = $1.2{\cdot}10^{-3}$ mol/dm^{-3} NMe_4Cl. λ_{ex}: 450 nm (except for Ni^{2+}: 462 nm). λ_{em}: 562 nm, + Mg^{2+} = 532 nm, + A, AE = 552 nm (+Mg^{2+} = 532 nm), + Zn^{2+} = 553 nm (+Mg^{2+} = 553 nm), + Cd^{2+} = 548 nm (+Mg^{2+} = 543 nm), Pb^{2+} = 553 nm (+Mg^{2+} = 553 nm). (For interpretation of the references to color in this figure legend, the reader is referred to the web version of this article.)

the same plane and a possible TICT quenching is prevented in this solvent. As a consequence, the enol emission is observed, even if low (Fig. 5, bottom; magenta lines).

In a neutral environment, in ACN (λ_{ex} 317 nm) **L2** and **L3** still showed very low emission, however with the keto band prevailing on the enol one (Fig. 5, top; black lines). On the contrary, the keto band of **L1** considerably increased, this is probably due to the presence of a small amount of the deprotonated HNBO form, as suggested by the UV–Vis spectrum (Fig. S3, top; black line). In other words, the deprotonated form seems to be responsible for the observed emission. In DMSO a low emission is observed for **L1** and **L2**, while **L3** showed the emission of the keto band (λ_{ex} 320 nm) (Fig. 5, bottom; black lines). Again, this increased emission goes along with the growth of the band of the deprotonated HNBO moiety observed in the absorption spectrum of **L3** (Fig. S3, bottom; black line).

The dependence of the emission from the presence of the deprotonated HNBO group is confirmed by the spectra of all ligands in both solvents in a basic environment (Fig. 5; violet lines), where a pronounced emission band (ACN: λ_{ex} 322 nm; DMSO: λ_{ex} 330 nm) is observed; this latter parallels the growth of the absorption band ascribable to the naphtholate moiety. It can be hypothesized that the deprotonation of the naphthol group allows for the delocalization of the negative charge on the whole HNBO system, increasing the electron density on the aromatic rings as well as the conjugation-induced coplanarity. These facts would, on one hand, prevent a possible PET effect from the amine functions, since an electron transfer from an amine lone pair towards an anionic emissive excited fluorophore is disfavored and, on the other hand, strengthen the coplanarity *via* an increased conjugation, causing the increase of the fluorescence emission.

The higher solubility of **L3** than **L1** and **L2** in aqueous solution allowed to investigate its acid-base behavior also in pure water (λ_{ex} at 317 nm) in the pH range 2–12, revealing different fluorescence properties at acidic pH values compared to ACN and DMSO but a similar behavior by moving towards basic pH values. From Fig. S4 it can be observed that, contrarily to what observed in organic solvents, at acidic pH values the equilibrium between keto and enol form is shifted towards the former, being the band of the keto form (λ_{em} at 555 nm) much higher than that of the enol form (λ_{em} at 425 nm), suggesting the occurrence of an ESIPT process in water. The emission of the keto form is then observed, possibly as a consequence of the formation of an intramolecular H bond that keeps the aromatic systems coplanar and thus prevents a possible TICT quenching. The emission of the ligand is substantially preserved up to pH 9 then, an increase of the emission and a blue-shift of the band from 555 to 540 nm is observed. The switching-ON of the fluorescence can be attributed to the deprotonation of the naphthol group as above discussed (*vide supra*).

3.3. Metal ions binding selectivity in DMSO

3.3.1. UV–Vis absorption and fluorescence behavior

The binding properties of **L1**–**L3** in DMSO solution towards A (Li^+, Na^+, K^+, Na^+, Cs^+), AE (Mg^{2+}, Ca^{2+}, Sr^{2+}, Ba^{2+}) as well as selected transition M^{2+} metal ions (Zn^{2+}, Cd^{2+}, Pb^{2+}, Cu^{2+}, Ni^{2+}) were investigated. UV–Vis (Fig. S5) and fluorescence (Fig. 6a) spectra of DMSO solutions containing $1.2{\cdot}10^{-5}$ mol/dm^{-3} **L1**–**L3** in the presence or absence of 1 equiv. of the metal ions were acquired. Moreover, the obtained maximum emission are reported as bar plots in Figs. 7 and Fig. S6.

Notably, among all tested cations, for all ligands the addition of 1 equiv. of Mg^{2+} induced the highest increase of the fluorescence emission; all other A and AE ions did not exhibit any significant variation of the emission of the ligand. In all cases, an enhancement of the fluorescence is observed also upon the addition of Zn^{2+} and Cd^{2+}: moreover, in these cases a quite different emission wavelength was observed (see fluorescence emission spectra and color of the solutions under a 360 nm UV lamp, Fig. 6), due to the different metal ions coordinated to the chemosensor compared to Mg^{2+}. Ni^{2+} and Cu^{2+} induced instead a quenching of the emission, as expected by the binding of these paramagnetic metal ions (Figs. 7 and Fig. S6).

The emission under a 360 nm laboratory UV lamp of the DMSO solutions of the ligands in the presence of some of the tested metal ions is depicted in Fig. 6b. The Mg^{2+}-containing solutions look clearly different from those containing Zn^{2+} and Cd^{2+}.

In other words, **L1**–**L3** show an interesting selectivity for Mg^{2+} in DMSO: in all cases, the whole UV–Vis spectrum of the free ligands undergoes a radical modification upon the addition of the metal ion suggesting the coordination of Mg^{2+} and the consequent deprotonation of the naphthol unit of the HNBO moiety (Fig. S5). The chromophore transition states are thus affected by the coordination of the cation and the fluorescence emission switches ON, with a new emission band resulting blue-shifted with respect to that of the keto band (Fig. S7). By using ESIPT-based chemosensors, a fluorescent ratiometric sensing may be possibly achieved, based on the ESIPT prevention upon metal ion coordination, resulting in enol fluorescence [35]. In the present case, no ratiometric response was observed (Fig. S7), so the fluorescence switch-ON must depend on other mechanisms. It can be suggested that the coordination of the metal ion on one hand prevents a possible PET effect

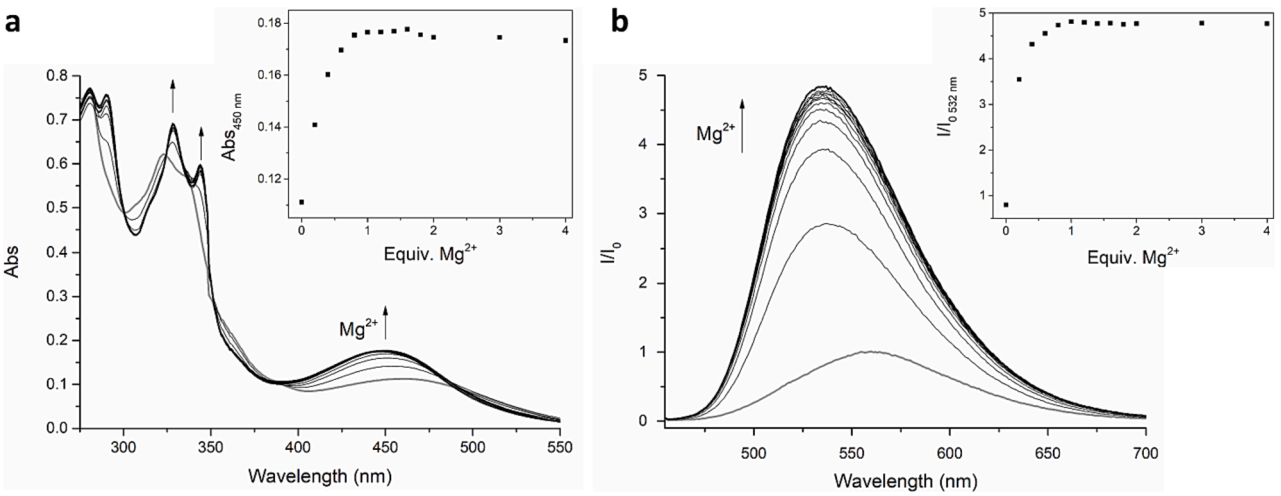

Fig. 8. UV–Vis absorption (a) and emission (b) spectra of **L3** in DMSO upon addition of up to 4 equiv. of Mg^{2+}. [**L3**] = $4.4{\cdot}10^{-5}$ mol/dm^{-3} in DMSO + 1.0 % H_2O, I = $4{\cdot}10^{-3}$ mol/dm^{-3} NMe_4Cl, λ_{ex} = 450 nm. Inset: a) trend of absorption at 450 nm as a function of equiv. of Mg^{2+} added; b) trend of emission at 532 nm as a function of equiv. of Mg^{2+} added.

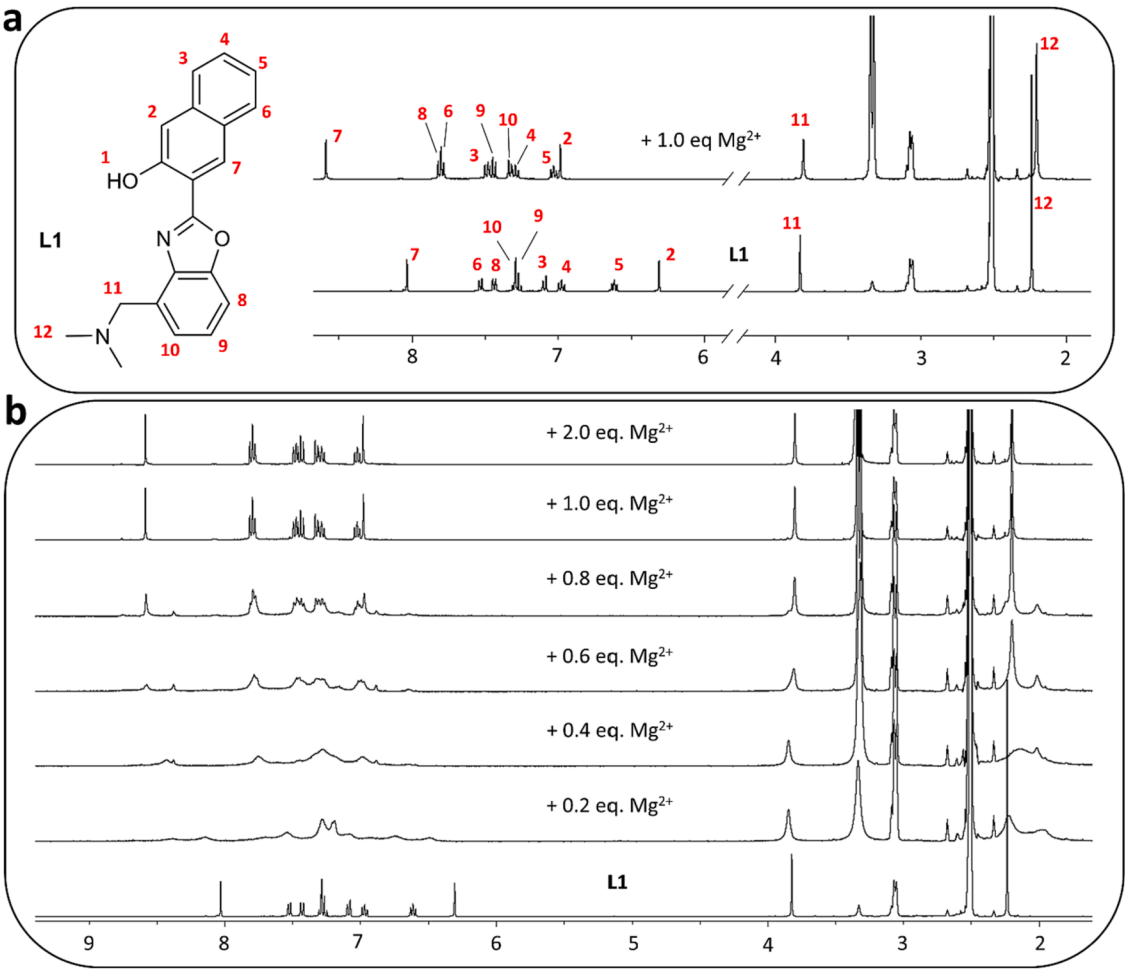

Fig. 9. A) numbering scheme of **L1** (left) and stack plot of ^{1}H NMR spectra of **L1** (in the presence of 1 equiv. of TMAOH) and magnesium complex in DMSO-d_6 (right); b) ^{1}H NMR spectra in DMSO-d_6 of **L1** upon sequential addition of up to 2 equiv. of Mg^{2+} ion (as perchlorate salt). [**L1**] = $1.0{\cdot}10^{-2}$ mol/dm^{-3}.

from the nitrogen lone-pair and, on the other hand, forces the aromatic systems to be co-planar, inhibiting a possible TICT quenching.

All other A and AE cations did not significantly affect either the UV–Vis absorption or the emission spectra of the ligands, suggesting the absence of guest coordination (Figs. S5, 6a). On the contrary, transition metal ions such as Zn^{2+} and Cd^{2+} induced great variations in the UV–vis absorption spectra, suggesting the formation of coordination species with **L1**–**L3** (Fig. S5); the fluorescence response to these cations is

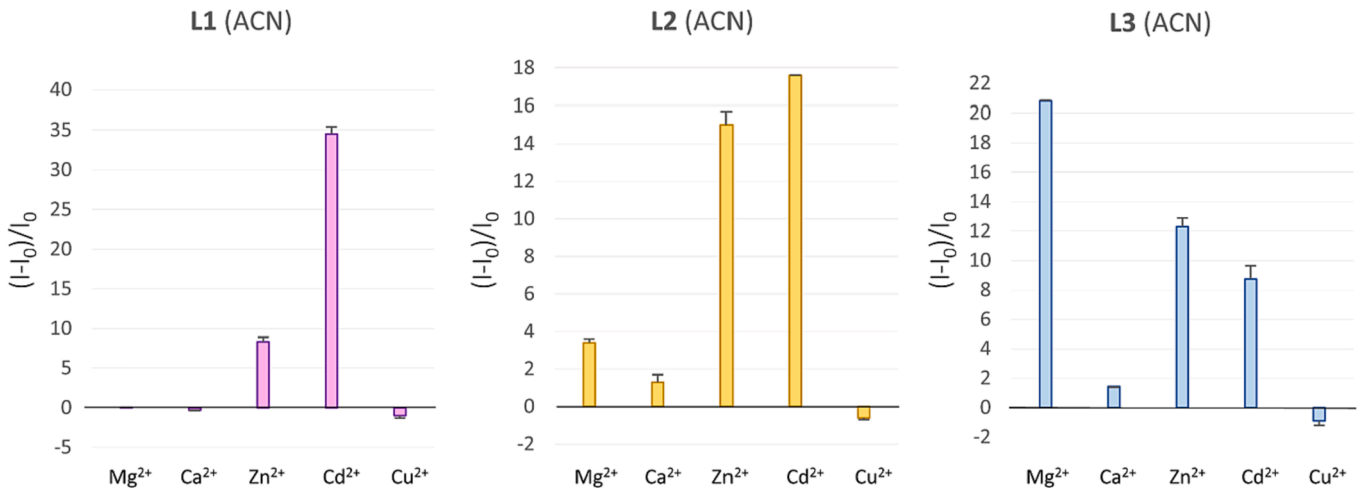

Fig. 10. Normalized maximum fluorescence emission of **L1**–**L3** upon addition of 1 equiv. of Mg^{2+}, Ca^{2+}, Zn^{2+}, Cd^{2+} and Cu^{2}. [**L**] = $1.2{\cdot}10^{-5}$ mol/dm^{-3} ACN + 1.0 % H_2O; $I = 1.2{\cdot}10^{-3}$ mol/dm^{-3} NMe_4Cl. λ_{ex}: 440 nm (**L1**-**L2**), 445 nm (**L3**); λ_{em}: 546 nm (**L1**-**L2**), 548 nm (**L3**); + Mg^{2+} = 535 nm (**L1**-**L2**), 531 nm (**L3**); + Zn^{2+} = 565 nm (**L1**-**L2**), 554 nm (**L3**); + Cd^{2+} = 560 nm (**L1**-**L2**), 554 nm (**L3**); + Ca^{2+} = 534 nm (**L1**–**L3**). λ_{ex}: 440 nm (**L1**-**L2**), 445 nm (**L3**); λ_{em}: 546 nm (**L1**-**L2**), 548 nm (**L3**); + Mg^{2+} = 535 nm (**L1**-**L2**), 531 nm (**L3**); + Zn^{2+} = 565 nm (**L1**-**L2**), 554 nm (**L3**); + Cd^{2+} = 560 nm (**L1**-**L2**), 554 nm (**L3**); + Ca^{2+} = 534 nm (**L1**–**L3**).

however lower than that observed to Mg^{2+} (Figs. 6, 7). A different DMSO solvation degree for Mg^{2+} and Zn^{2+}/Cd^{2+} could be the reason for this different behavior, so that notwithstanding the coordination of Zn^{2+} and Cd^{2+} to **L1**–**L3**, the binding is less efficient and a possible partial PET effect from the nitrogen lone pair could affect the emission. In the case of paramagnetic ions such as Cu^{2+} and Ni^{2+}, a deep modification of the UV–Vis absorption spectra is observed in all cases (Fig. S5), together with an expected quenching of the fluorescence (Figs. 6, 7).

3.3.2. *UV–Vis, fluorescence and ^{1}H NMR titrations with Mg^{2+}*

Due to the marked CHEF effect observed for all ligands in the presence of Mg^{2+}, the binding behavior towards this metal ion in DMSO was investigated more in depth by UV–Vis, fluorescence and ^{1}H NMR titrations.

The UV–vis absorption titrations of **L1**, **L2** and **L3** with Mg^{2+} in DMSO showed the growth of a new band at 444 nm (**L1**, **L2**) or the increase of the existing small band at 462 nm and its blue-shift to 450 nm (**L3**), attributable to the involvement of the naphthol oxygen atom in the Mg^{2+} coordination inducing the naphthol deprotonation (Fig. S8a, Fig. S9a, 8a for **L1**, **L2** and **L3**, respectively). The emission intensity following the addition of Mg^{2+} also increased (see Table S2 and Fig. S8b, Fig. S9b, 8b for **L1**, **L2** and **L3**, respectively). In all cases, the results of both absorption and emission titrations are in good agreement. In the case of **L1** and **L2**, firstly the formation of a species with a 2:1 ligand to Mg^{2+} molar ratio can be suggested, until a deficiency of Mg^{2+} is present in the solution, secondly a species with a 1:1 ligand to Mg^{2+} molar ratio formed in solution (Figs. S8, S9). In the case of **L3**, the formation of a 1:1 species is observed in solution (Fig. 8).

^{1}H NMR titrations of the ligands with Mg^{2+} in DMSO-d_6 (Figs. 9, S10, S11 for **L1**, **L2** and **L3**, respectively) confirmed in all cases both the formation of Mg^{2+}-complexes as well as the stoichiometries observed from UV–vis measurements. All ligand solutions were added of an

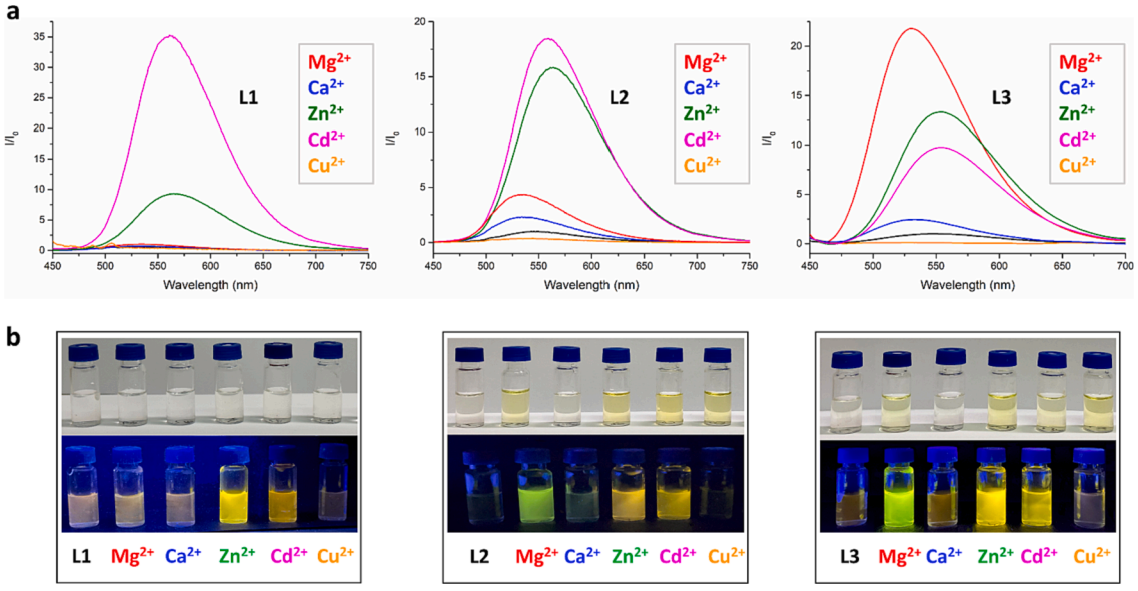

Fig. 11. a) Emission spectra of **L1**–**L3** upon the addition of 1 equiv. of A, AE and transition metal ions in ACN. b) Color change (top) and enhancement of the fluorescence under a 360 nm UV lamp (bottom) of **L1**, **L2** and **L3** ACN solutions before and after the addition of 1 equiv. of Mg^{2+}, Ca^{2+}, Zn^{2+}, Cd^{2+}, Cu^{2+}. [**L**] = $1.2{\cdot}10^{-5}$ mol/dm^{-3} ACN + 1.0 % H_2O; $I = 1.2{\cdot}10^{-3}$ mol/dm^{-3} NMe_4Cl. λ_{ex}: 440 nm (**L1**-**L2**), 445 nm (**L3**); λ_{em}: 546 nm (**L1**-**L2**), 548 nm (**L3**); + Mg^{2+} = 535 nm (**L1**-**L2**), 531 nm (**L3**); + Zn^{2+} = 565 nm (**L1**-**L2**), 554 nm (**L3**); + Cd^{2+} = 560 nm (**L1**-**L2**), 554 nm (**L3**); + Ca^{2+} = 534 nm (**L1**–**L3**).

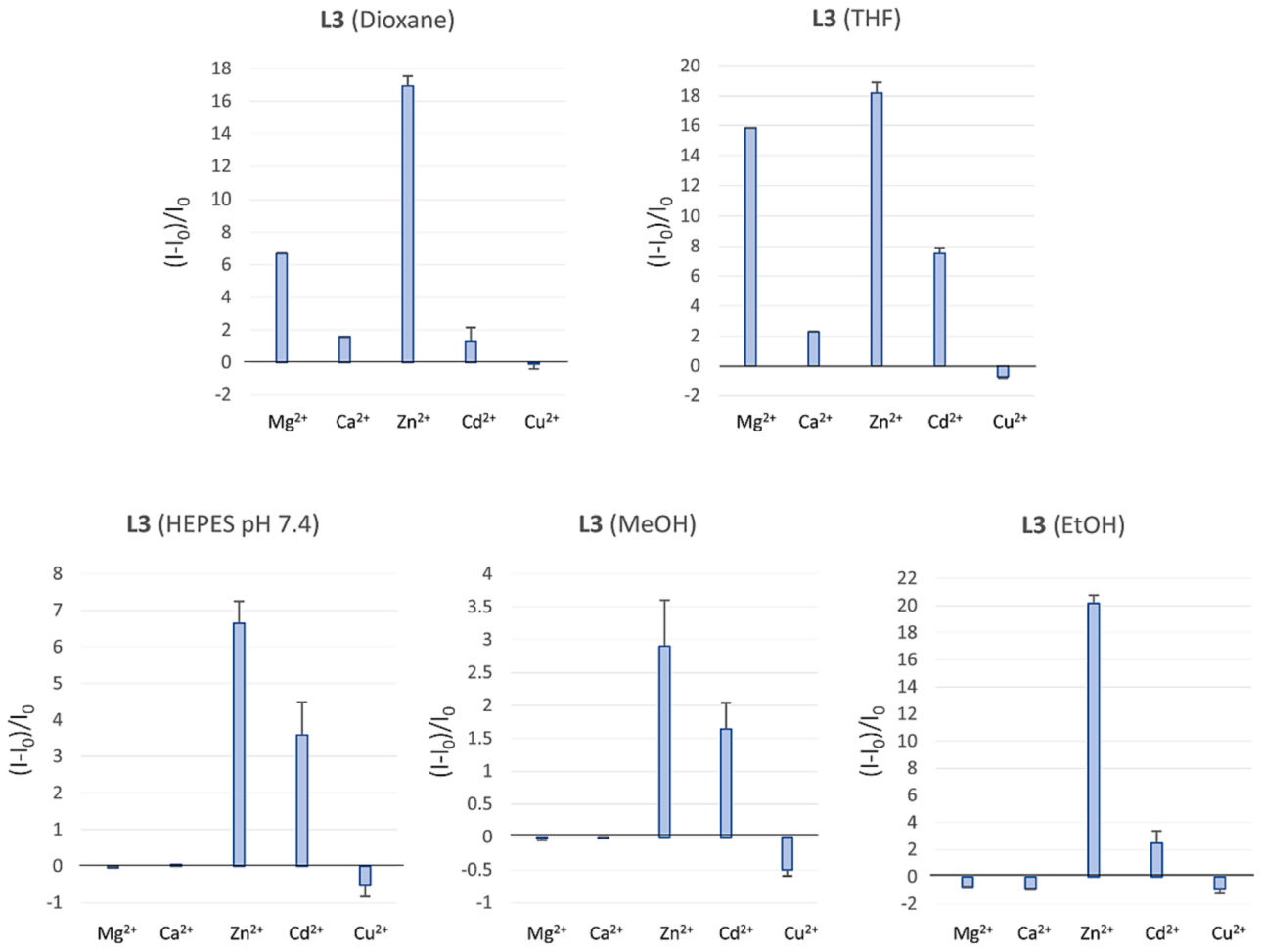

Fig. 12. Normalized maximum fluorescence emission of **L3** upon addition of 1 equiv. of Mg^{2+}, Ca^{2+}, Zn^{2+}, Cd^{2+} and Cu^{2+} in THF, dioxane, H_2O (HEPES pH 7.4), MeOH and EtOH. [**L**] = $1.2{\cdot}10^{-5}$ mol/dm^{-3} in the different solvents (+1.0 % H_2O); $I = 1.2{\cdot}10^{-3}$ mol/dm^{-3} NMe_4Cl. λ_{ex}: 445 nm; λ_{em}. THF: 546 nm, + Mg^{2+} = 539 nm, + Ca^{2+} = 544 nm, + Zn^{2+} = 555 nm, + Cd^{2+} = 561 nm; dioxane: 551 nm, + Mg^{2+} = 539 nm, + Ca^{2+} = 554 nm, + Zn^{2+} = 560 nm, + Cd^{2+} = 540 nm; H_2O: 539 nm, + Mg^{2+} = 540 nm, + Ca^{2+} = 533 nm, + Zn^{2+} = 542 nm, + Cd^{2+} = 544 nm; + Cu^{2+} = 530 nm; MeOH: 549 nm, + Mg^{2+} = 546 nm, + Ca^{2+} = 548 nm, + Zn^{2+} = 551 nm, + Cd^{2+} = 550 nm; + Cu^{2+} = 552 nm; EtOH: 543 nm, + Zn^{2+} = 549 nm, + Cd^{2+} = 550 nm.

equimolar amount of TMAOH (1 eq. for **L1**; 3 eq. for **L2·2HCl**; 4 eq. for **L3·3HCl**).

In all cases, upon the addition of Mg^{2+} firstly the broadening of all the resonances is observed, suggesting the presence of two species slowly exchanging on the NMR time scale, with most signals shifting down-field, highlighting the binding of Mg^{2+}. When the addition of 1 equiv. of Mg^{2+} is reached, only one species featuring sharp peaks is present in solution and no changes were observed upon the addition of further metal ion.

These results suggest the formation of a 1:1 ligand to metal ion complex species for all ligands. In the case of **L1** and **L2**, the formation of an intermediate 2:1 ligand to metal ion species can be suggested until an excess of ligand compared to metal cation is present in solution (Figs. 9, S10), confirming the UV–Vis and fluorescence results.

In all cases, the aromatic fluorophore moiety results to be involved in the coordination of Mg^{2+}, due to both the observed resonances shifts and the changes in the absorption and emission spectra of all three chemosensors upon the addition in solution of the metal cation. Also, the polyamine fragment of all ligands seems to be involved in the coordination of Mg^{2+}, due to the shifts and/or splitting of the aliphatic resonances in the ^{1}H NMR spectra. Featuring the simplest structure among the three compounds, **L1** does not show any splitting of the aliphatic signals, as it is instead observed for **L2**, that possesses a longer polyamine chain: the singlet attributed to the H11 resonance of **L2** splitted indeed into a characteristic AB system due to two nonequivalent protons of the benzylic –CH_2 group (Fig. S10), suggesting the stiffening of the system upon Mg^{2+} ion complexation as well as the involvement of the aliphatic polyamine in the coordination.

3.3.3. *Ion competition studies*

Ion competition studies in DMSO were performed by UV–Vis and fluorescence measurements by adding 1 equiv. of Mg^{2+} to solutions of **L1**, **L2** and **L3** containing A, AE or transition metal ions in equimolar amounts (Figs. 7, S6).

In the case of **L1**, the addition of Mg^{2+} in the presence of A and AE revealed a partial interference of these cations in the coordination of Mg^{2+}, since the emission obtained upon the addition of Mg^{2+} did not reach the same emission of the magnesium complex (Fig. S6). On the contrary, the addition of A and AE did not seem to influence the fluorescence response to Mg^{2+} of both **L2** and **L3** (Fig. S6, 7).

In all cases, Zn^{2+}, Cd^{2+} and Pb^{2+} showed to compete with Mg^{2+} for the coordination to the ligands, since the addition of Mg^{2+} caused no to slight variation of the emission of the complexes. Finally, in the presence of Ni^{2+} and Cu^{2+}, the addition of Mg^{2+} did not cause, as expected, the switch-ON of the chemosensors, suggesting total interference of the paramagnetic ions in the response of **L1**–**L3** to Mg^{2+} (Figs. 7, S6).

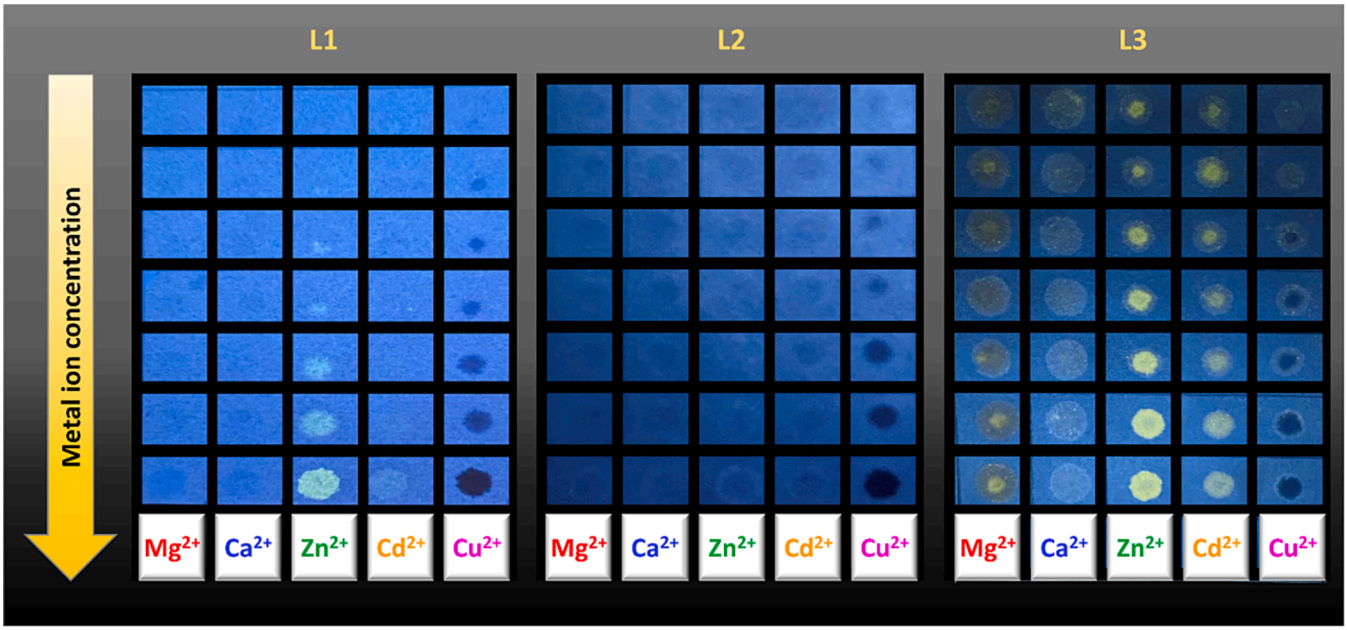

Fig. 13. Paper strip test: filter papers immersed in **L1**–**L3** solutions in ACN on which 1 μl of metal ion solution at growing concentrations (from top to bottom: $5{\cdot}10^{-5}$, $2.5{\cdot}10^{-4}$, $5{\cdot}10^{-4}$, $1{\cdot}10^{-3}$, $5{\cdot}10^{-3}$, $1{\cdot}10^{-2}$, $5{\cdot}10^{-2}$ mol/dm^{-3}) was deposited. All paper strips were observed under a UV lamp at 360 nm.

3.4. Metal ions selectivity in ACN

The fluorescence selectivity of **L1**–**L3** towards selected metal ions was also verified in ACN. In Fig. 10 are depicted the enhancements in fluorescence intensity of the three ligands in ACN upon the addition of Mg^{2+}, Ca^{2+}, Zn^{2+}, Cd^{2+} and Cu^{2+}, while in Fig. 11a are shown the corresponding emission spectra. Interestingly, compared to DMSO, the selectivity of **L1** and **L2** in ACN is shifted towards Zn^{2+} and Cd^{2+} rather than Mg^{2+}. On the other hand, **L3** maintained the selectivity towards Mg^{2+} also in ACN, and, notably, again its response to Mg^{2+} is higher than that to Zn^{2+} and Cd^{2+}. In Fig. 11b the emission under a 360 nm laboratory UV lamp of the ACN solutions of the ligands in the presence of the tested metal ions is also shown: clearly, **L1** is selective for Zn^{2+} and Cd^{2+}, while **L2** and **L3** can signal both Mg^{2+} and Zn^{2+} and Cd^{2+}, but the solutions containing Mg^{2+} are quite recognizable from the different color emission.

The addition of Mg^{2+} did not perturb the UV–Vis absorption spectrum of **L1** in ACN while spectral changes were observed upon the addition of Mg^{2+} to **L2** and **L3** (Fig. S12). The addition of Zn^{2+} affected the absorption of both **L2** and **L3** and, to a lesser extent, **L1**, while the addition of Cd^{2+} and Cu^{2+} always induced a deep change of all spectra (Fig. S12). These results suggest that all ligands form complexes with transition metal ions, while only **L2** and **L3** are able to bind Mg^{2+}. However, the fluorescence response to Mg^{2+} of **L3** is higher than that of **L2**: it can be hypothesized that the complexation of Mg^{2+} by **L3** overcomes the solvation energies that probably totally or partially impair the complex formation in the case of **L1** and **L2**.

3.5. Metal ions selectivity in other solvents

Besides ACN and DMSO, the binding ability of **L3** towards Mg^{2+}, Ca^{2+}, Zn^{2+}, Cd^{2+} and Cu^{2+} was studied also in water (HEPES buffer pH 7.4), dioxane, THF, methanol (MeOH) and ethanol (EtOH) (Figs. 12, S13, S14).

L3 proved able to give a fluorescence response to Mg^{2+} in several solvents among those tested. As already discussed, in DMSO (Fig. 7) and ACN (Fig. 10) the response to Mg^{2+} is quite selective, being higher than that to any other cation, while in THF and dioxane the response to Mg^{2+} is lower than that to Zn^{2+} (Fig. 12, top).

In the protic solvents (water, MeOH and EtOH) **L3** did not show any fluorescence response to Mg^{2+}, in line with a strong solvation of Mg^{2+} in those conditions. In such solvents the selectivity is instead shifted towards Zn^{2+} and Cd^{2+}, being totally selective for Zn^{2+} in EtOH (Fig. 12, bottom).

3.6. Metal detection on a solid support

The development of a green, easy and rapid qualitative procedure to assess the presence of metal cations in a solution sample could be of interest. To this purpose, the sensing procedure was moved from the solution environment to a solid support by performing a paper strip test, which could possibly allow for the fast qualitative detection of the guests in a sample *via* a fluorescence signal by using a common UV laboratory lamp.

To assess the system, simple filter paper strips were immersed in an ACN solution of each ligand ([**L**] = $1{\cdot}10^{-4}$ mol/dm^{-3}) for a few minutes; after complete drying, guest solutions with increasing concentrations were deposited as small drops on the paper, and, finally, the paper strips were observed under a UV lamp (λ_{ex} 360 nm).

As can be observed in Fig. 13, the ability to detect metal ions moving from the solution studies to the paper support changes among the series of ligands. **L2** is the worst performing sensor on the solid support, while **L1** and **L3** showed good results. In particular, **L1** is able to detect Zn^{2+} while **L3** responds to Zn^{2+}, Cd^{2+} and Mg^{2+}, confirming the signaling properties of the two ligands observed in ACN solutions. In all cases, Cu^{2+} quenches the emission of the ligand even on the paper support.

4. Conclusion

In this paper, a family of three HNBO-based fluorescent chemosensors has been designed and synthesized with a growing structural complexity by changing the aliphatic polyamine scaffold linked to a HNBO moiety.

As possible ESIPT-based chemosensors, the three ligands were studied in different solvents by UV–Vis and fluorescence spectroscopies, revealing the occurrence of the ESIPT process in ACN and the prevention of the ESIPT process in DMSO, that, being more basic and containing a higher number of donor atoms, could better interact with the –OH

naphthol group enabling the enol emission. **L3** represents an exception, featuring an ESIPT process in both aprotic solvents. Notably, the ESIPT process in **L3** also occurs in protic solvents (water and EtOH-10 % water mixture), while it is prevented in EtOH: the H-bond formation between the organic solvent and water, or between water molecules, seems thus to be favored compared to the interaction between the chemosensor and the solvent, enabling the ESIPT process.

The study of the acid-base behavior revealed that in an acidic environment all ligands are very low emissive in ACN (TICT quenching) while a low enol emission is observed in DMSO (TICT prevention). In a neutral environment, only **L1** is emissive in ACN, while only **L3** is emissive in DMSO: in both cases, the emission is relative to the deprotonated form of the ligand. This last statement is confirmed by both the fact that in a basic environment the emission of all ligands is switched-ON in both solvents as well as a strong emission is also observed for **L3** in aqueous solution above pH 9 (PET and TICT prevention).

Notwithstanding the ESIPT-allowing structure, all chemosensors did not feature an ESIPT-based signaling ability towards A, AE and some transition metal ions, neither in ACN nor in DMSO. The prevention of both a PET effect and a TICT quenching could be suggested as a possible mechanism for the observed switch-ON.

UV–vis spectrophotometric and spectrofluorimetric measurements revealed that **L1**–**L3** show an interesting selectivity for Mg^{2+} in DMSO, with the formation of emissive Mg^{2+}-complexes with 2:1 (in excess of **L1** and **L2**) and 1:1 ligand to metal ion stoichiometries, confirmed by NMR titrations. In ACN the selectivity shifts towards Zn^{2+} and Cd^{2+}, except for **L3**, that still shows the highest fluorescence response to Mg^{2+}. **L3** is also able to respond to Mg^{2+} in other aprotic solvents (THF and dioxane), but with a lower selectivity, while it only responds to Zn^{2+} and Cd^{2+} in protic solvents (water, MeOH and EtOH).

Finally, a paper strip test revealed that **L1** can detect Zn^{2+} while **L3** can detect Zn^{2+}, Cd^{2+} and Mg^{2+} even on a paper support. Interestigly, **L3** revealed able to signal the presence of Mg^{2+} both in solution, in different solvents, as well as on a paper support.

CRediT authorship contribution statement

Daniele Paderni: Investigation. **Daniele Lopez:** Investigation. **Eleonora Macedi:** Conceptualization, Validation, Supervision, Writing – original draft. **Gianluca Ambrosi:** Investigation. **Angela Ricci:** Investigation. **Erika Palazzetti:** Investigation. **Luca Giorgi:** Writing – review & editing. **Mauro Formica:** Investigation, Writing – review & editing. **Vieri Fusi:** Conceptualization, Supervision, Writing – review & editing.

Declaration of Competing Interest

The authors declare that they have no known competing financial interests or personal relationships that could have appeared to influence the work reported in this paper.

Data availability

Data will be made available on request.

Acknowledgements

Ms Anna Rita Pierleoni is greatly acknowledged for her help with NMR measurements. This work was financially supported by the Italian Ministero dell'Istruzione dell'Università e della Ricerca (MIUR – project 2017EKCS35) and by the University of Urbino (Grant DISPEA_ASSEGNAZIONE_ATENEO_SICUREZZA_ALIMENTARE, DISPEA_MACEDI_PROG21).

Appendix A. Supplementary data

Supplementary data to this article can be found online at https://doi.org/10.1016/j.ica.2023.121400.

References

[1] C.A. Brautigam, T.A. Steitz, Structural and functional insights provided by crystal structures of DNA polymerases and their substrate complexes, Curr. Opin. Struct. Biol. 8 (1998) 54–63, https://doi.org/10.1016/S0959-440X(98)80010-9.
[2] W. Chul Suh, S. Leirmo, M. Thomas Record Jr., Roles of magnesium in the mechanism of formation and dissociation of open complexes between Escherichia coli RNA polymerase and the .lambda.PR promoter: kinetic evidence for a second open complex requiring magnesium, Biochemistry. 31 (2002) 7815–7825. 10.1021/bi00149a011.
[3] R. Caspi, R. Billington, I.M. Keseler, A. Kothari, M. Krummenacker, P.E. Midford, W.K. Ong, S. Paley, P. Subhraveti, P.D. Karp, The MetaCyc database of metabolic pathways and enzymes – a 2019 update, Nucleic Acids Res. 48 (2020) D445–D453. 10.1093/NAR/GKZ862.
[4] K. Mubagwa, A. Gwanyanya, S. Zakharov, R. Macianskiene, Regulation of cation channels in cardiac and smooth muscle cells by intracellular magnesium, Arch. Biochem. Biophys. 458 (2007) 73–89, https://doi.org/10.1016/J.ABB.2006.10.014.
[5] P. Paoletti, C. Bellone, Q. Zhou, NMDA receptor subunit diversity: impact on receptor properties, synaptic plasticity and disease, Nat. Rev. Neurosci. 2013 146. 14 (2013) 383–400. 10.1038/nrn3504.
[6] A.C. Alfrey, N.L. Miller, R. Trow, Effect of age and magnesium depletion on bone magnesium pools in rats, J. Clin. Invest. 54 (1974) 1074–1081, https://doi.org/10.1172/JCI107851.
[7] F. Mammoli, S. Castiglioni, S. Parenti, C. Cappadone, G. Farruggia, S. Iotti, P. Davalli, J.A.M. Maier, A. Grande, C. Frassineti, Magnesium Is a Key Regulator of the Balance between Osteoclast and Osteoblast Differentiation in the Presence of Vitamin D3, Int. J. Mol. Sci. 2019, 20, Page 385. 20 (2019) 385. 10.3390/IJMS20020385.
[8] W.C. Lu, E. Pringa, L. Chou, Effect of magnesium on the osteogenesis of normal human osteoblasts, Magnes. Res. 30 (2017) 42–52, https://doi.org/10.1684/MRH.2017.0422.
[9] M.E. Shils, Experimental human magnesium depletion, Med. (United States) 48 (1969) 61–85, https://doi.org/10.1097/00005792-196901000-00003.
[10] D. Fiorentini, C. Cappadone, G. Farruggia, C. Prata, Magnesium: biochemistry, nutrition, detection, and social impact of diseases linked to its deficiency, Nutrients. 13 (2021) 1136, https://doi.org/10.3390/NU13041136.
[11] J.H.F. de Baaij, J.G.J. Hoenderop, R.J.M. Bindels, Magnesium in man: Implications for health and disease, Physiol. Rev. 95 (2015) 1–46, https://doi.org/10.1152/PHYSREV.00012.2014/ASSET/IMAGES/LARGE/Z9J0041427110008.JPEG.
[12] J. Feng, H. Wang, Z. Jing, Y. Wang, Y. Cheng, W. Wang, W. Sun, Role of magnesium in type 2 diabetes mellitus, (2011). 10.1007/s12011-019-01922-0.
[13] I. Zofkova, M. Davis, J. Blahos, Trace elements have beneficial, as well as detrimental effects on bone homeostasis, Physiol. Res. 66 (2017) 391–402. 10.33549/physiolres.933454.
[14] A.E. Kirkland, G.L. Sarlo, K.F. Holton, The Role of Magnesium in Neurological Disorders, Nutr. 2018, Vol. 10, Page 730. 10 (2018) 730. 10.3390/NU10060730.
[15] S.M.G. Al-Ghamdi, E.C. Cameron, R.A.L. Sutton, Magnesium deficiency: pathophysiologic and clinical overview, Am. J. Kidney Dis. 24 (1994) 737–752, https://doi.org/10.1016/S0272-6386(12)80667-6.
[16] I. of Medicine, Dietary Reference Intakes for Calcium, Phosphorus, Magnesium, Vitamin D, and Fluoride, 1997, https://doi.org/10.17226/5776.
[17] L. Lvova, C.G. Gonçalves, C. Di Natale, A. Legin, D. Kirsanov, R. Paolesse, Recent advances in magnesium assessment: From single selective sensors to multisensory approach, Talanta 179 (2018) 430–441, https://doi.org/10.1016/j.talanta.2017.11.019.
[18] E.W. Rice, R.B. Baird, A.D. Eaton, Standard Methods for the Examination of Water and Wastewater, 23rd Edition, American Public Health Association, American Water Works Association, Water Environment Federation, 2017.
[19] J.-M. Peng, H.-L. Wang, Z.-H. Zhu, Z.-Y. Liu, H.-H. Zou, F.-P. Liang, Substituents lead to differences in the formation of a series of dysprosium hydrogen-bonded organic frameworks with high stability and acid stimulus-response luminescence properties, J. Mater. Chem. C. 9 (2021) 9319–9330, https://doi.org/10.1039/d1tc01672e.
[20] Y.L. Li, H.L. Wang, Z.C. Chen, Z.H. Zhu, Y.C. Liu, R.Y. Yang, F.P. Liang, H.H. Zou, Lanthanoid hydrogen-bonded organic frameworks: Enhancement of luminescence by the coordination-promoted antenna effect and applications in heavy-metal ion sensing and sterilization, Chem. Eng. J. 451 (2023), 138880, https://doi.org/10.1016/J.CEJ.2022.138880.
[21] E. Arunkumar, P. Chithra, A. Ajayaghosh, A controlled supramolecular approach toward cation-specific chemosensors: Alkaline earth metal ion-driven exciton signaling in squaraine tethered podands, J. Am. Chem. Soc. 126 (2004) 6590–6598, https://doi.org/10.1021/JA0393776/SUPPL_FILE/JA0393776SI20040315_102304.PDF.
[22] H. Komatsu, N. Iwasawa, D. Citterio, Y. Suzuki, T. Kubota, K. Tokuno, Y. Kitamura, K. Oka, K. Suzuki, Design and synthesis of highly sensitive and selective fluorescein-derived magnesium fluorescent probes and application to intracellular 3D Mg2+ imaging, J. Am. Chem. Soc. 126 (2004) 16353–16360, https://doi.org/10.1021/ja049624l.

[23] M. Patil, K. Keshav, M.K. Kumawat, S. Bothra, S.K. Sahoo, R. Srivastava, J. Rajput, R. Bendre, A. Kuwar, Monoterpenoid derivative based ratiometric fluorescent chemosensor for bioimaging and intracellular detection of Zn2+ and Mg2+ ions, J. Photochem. Photobiol. A Chem. 364 (2018) 758–763, https://doi.org/10.1016/J.JPHOTOCHEM.2018.07.015.

[24] V.N. Tuan, T.D. Dinh, W. Zhang, A.M. Khattak, A.T. Le, I.A. Saeed, W. Gao, M. Wang, A smart diagnostic tool based on deep kernel learning for on-site determination of phosphate, calcium, and magnesium concentration in a hydroponic system, RSC Adv. 11 (2021) 11177–11191, https://doi.org/10.1039/D1RA00140J.

[25] Y. Li, M.Y. Chi, A tryptophan-containing open-chain framework for tuning a high selectivity for Ca2+ and 13C NMR observation of a Ca 2+-indole interaction in aqueous solution, J. Am. Chem. Soc. 127 (2005) 3527–3530, https://doi.org/10.1021/JA046517I/SUPPL_FILE/JA046517ISI20041026_065424.PDF.

[26] K.C. Song, M.G. Choi, D.H. Ryu, K.N. Kim, S.K. Chang, Ratiometric chemosensing of Mg2+ ions by a calix[4]arene diamide derivative, Tetrahedron Lett. 48 (2007) 5397–5400, https://doi.org/10.1016/J.TETLET.2007.06.010.

[27] S.H. Mashraqui, S. Sundaram, A.C. Bhasikuttan, S. Kapoor, A.V. Sapre, Novel fluoroionophores incorporating diaryl-1,3,4-oxadiazole and aza-crown ring. Potentially sensitive Mg2+ ion sensor, Sensors Actuators B Chem. 122 (2007) 347–350, https://doi.org/10.1016/J.SNB.2006.07.010.

[28] M. Ishida, Y. Naruta, F. Tani, M. Ishida, Y. Naruta, F. Tani, Molecular recognition A porphyrin-related macrocycle with an embedded 1,10-phenanthroline moiety: fluorescent magnesium(II) ion sensor, Angew. Chem. Int. Ed. 49 (2010) 91–94, https://doi.org/10.1002/anie.200904859.

[29] Y. Ma, H. Liu, S. Liu, R. Yang, A simple fluorescent receptor selective for Mg2+, Analyst. 137 (2012) 2313–2317, https://doi.org/10.1039/c2an35200a.

[30] S. Amatori, G. Ambrosi, M. Fanelli, M. Formica, V. Fusi, L. Giorgi, E. Macedi, M. Micheloni, P. Paoli, P. Rossi, A preorganized metalloreceptor for alkaline earth ions showing calcium versus magnesium selectivity in water: Biological activity of selected metal complexes, Chem. - A Eur. J. 20 (2014) 11048–11057, https://doi.org/10.1002/chem.201403084.

[31] Y. Li, J. Wu, X. Jin, J. Wang, S. Han, W. Wu, J. Xu, W. Liu, X. Yao, Y. Tang, A bimodal multianalyte simple molecule chemosensor for Mg2+, Zn2+, and Co2+, Dalt. Trans. 43 (2014) 1881–1887, https://doi.org/10.1039/C3DT52618F.

[32] L. Li, S. Yun, Z. Yuan-Hui, M. Lan, Z. Xi, C. Redshaw, W. Gang, A single chemosensor for multiple analytes: fluorogenic and ratiometric absorbance detection of Zn2+, Mg2+ and F−, and its cell imaging, Sensors Actuators B Chem. 226 (2016) 279–288, https://doi.org/10.1016/J.SNB.2015.11.126.

[33] D. Paderni, E. Macedi, L. Lvova, G. Ambrosi, M. Formica, L. Giorgi, R. Paolesse, V. Fusi, Selective detection of Mg2+ for sensing applications in drinking water, Chem. - A Eur. J. 28 (2022), https://doi.org/10.1002/chem.202201062.

[34] A. Garau, L. Lvova, E. Macedi, G. Ambrosi, M.C. Aragoni, M. Arca, C. Caltagirone, S.J. Coles, M. Formica, V. Fusi, L. Giorgi, F. Isaia, V. Lippolis, J.B. Orton, R. Paolesse, N2S2pyridinophane-based fluorescent chemosensors for selective optical detection of Cd2+in soils, New J. Chem. 44 (2020) 20834–20852, https://doi.org/10.1039/d0nj03858j.

[35] J. Eon Kwon, S. Lee, Y. You, K.-H. Baek, K. Ohkubo, J. Cho, S. Fukuzumi, I. Shin, S. Young Park, W. Nam, Fluorescent zinc sensor with minimized proton-induced interferences: photophysical mechanism for fluorescence turn-on response and detection of endogenous free zinc ions, Inorg. Chem. 51 (2012) 8760–8774, https://doi.org/10.1021/ic300476e.

[36] L. He, C. Liu, J.H. Xin, A novel turn-on colorimetric and fluorescent sensor for Fe3+ and Al3+ with solvent-dependent binding properties and its sequential response to carbonate, Sensors Actuators B Chem. 213 (2015) 181–187, https://doi.org/10.1016/J.SNB.2015.02.060.

[37] H. Kobayashi, K. Katano, T. Hashimoto, T. Hayashita, Solvent effect on the fluorescence response of hydroxycoumarin bearing a dipicolylamine binding site to metal ions, Anal. Sci. 30 (11) (2014) 1045–1050.

[38] G.H. Searle, S.F. Lincoln, S.G. Teague, D.G. Rowe, Cobalt(111) Complexes with QMethyldiethylene- triamine [2,2'-Methyliminodi(ethy1amine)l: Their Separation, Characterization and Reactions, Synthesis (Stuttg) 32 (1979) 519–536.

[39] A.C. Sedgwick, L. Wu, H.H. Han, S.D. Bull, X.P. He, T.D. James, J.L. Sessler, B. Z. Tang, H. Tian, J. Yoon, Excited-state intramolecular proton-transfer (ESIPT) based fluorescence sensors and imaging agents, Chem. Soc. Rev. 47 (2018) 8842–8880, https://doi.org/10.1039/c8cs00185e.

[40] S. Barman, S.K. Mukhopadhyay, M. Gangopadhyay, S. Biswas, S. Dey, N.D. P. Singh, Coumarin-benzothiazole-chlorambucil (Cou-Benz-Cbl) conjugate: An ESIPT based pH sensitive photoresponsive drug delivery system, J. Mater. Chem. B 3 (2015) 3490–3497, https://doi.org/10.1039/c4tb02081b.

[41] K.V. Gensh, Y.E. Zevatskii, D.V. Samoylov, S.V. Shekhovtsov, A.V. Lebed, S. T. Goga, N.O. Mchedlov-Petrossyan, Ionic equilibrium in mixtures of polar protophobic and protophilic non-hydrogen bond donor solvents: Acids, salts, and indicators in acetonitrile with 4 mass % dimethylsulfoxide, J. Mol. Liq. 322 (2021), 114560, https://doi.org/10.1016/j.molliq.2020.114560.